MIRI IFU and NIRSpec Observations of Cas A

This article details a science use case that involves an IFU observing scenario using NIRSpec and MIRI in parallel to observe a supernova remnant.

Introduction

Cassiopeia A ("Cas A") is a supernova remnant (SNR) located in our Galaxy that is estimated to have erupted approximately in the year 1680 C.E. (Fesen et al., 1988). Because it is in our Galaxy, it makes for an excellent laboratory to study SNRs in detail. The diameter of the shell of the remnant as can be measured from Spitzer IRAC images is ~3.7 arcminutes. Supernovae are important players in the life cycle of matter in a galaxy (for studies of nearby galaxies, see: Milky Way, Draine 2009; Large Magellanic Cloud, Matsuura et al., 2009; Small Magellanic Cloud, Boyer et al., 2012), so studying a nearby one such as Cas A is important for understanding how supernovae contribute to the galactic life cycle of matter.

Among the more interesting features within the SNR are what are known as "Fast Moving Knots", or FMKs. These are clumps of freshly-synthesized material in the SNR (Douvion et al 2001). Spectroscopy at optical (Hurford & Fesen 1996), near-infrared (Gerardy & Fesen 2001), and mid-infrared (Douvion et al., 2001; Ennis et al., 2006; Rho et al., 2008) wavelengths of these FMKs show evidence for emission from both atomic and solid-state material.

Instruments and modes used for science

See also: MIRI Medium Resolution Spectroscopy, NIRSpec IFU Spectroscopy, JWST Parallel Observations

This observation will observe FMKs 1, 2, and 3 from Hurford & Fesen (1996) in the northern parts of the Cas A SNR using both NIRSpec and MIRI IFUs. The NIRSpec IFU would obtain 2 × 2 mini-mosaics, since the NIRSpec IFU is only 3" × 3". For MIRI-MRS, only 1 pointing will be obtained for each FMK (no mini-mosaic), plus a single dedicated background obtained from nearby sky. This is making use of an on-source/off-source strategy (see JWST ETC IFU Nod in Scene and IFU Nod off Scene Strategy): one observation for each of the 3 targets, followed by a sky observation to be used for sky subtraction. All pointings will use a 4-dither pattern (see MIRI MRS Dithering and NIRSpec IFU Dither and Nod Patterns). The NIRSpec IFU will be used in the highest spectral resolution mode (R ~ 2700) (see NIRSpec Dispersers and Filters), in order to begin to resolve the velocity structure of the lines in a manner not possible with, for instance, the Short-High or Long-High modules on Spitzer-IRS (both have R ~ 600). Both the NIRSpec IFU and MIRI-MRS have much higher spatial resolution (~0.1" pixels) than Spitzer-IRS (~1.8" pixels in Short-Low) or even Spitzer-IRAC (~1.2" pixels).

Exposure Time Calculator

See also: Exposure Time Calculator, JWST ETC Scenes and Sources Page Overview

Spectra were obtained using the CUBISM tool (Smith et al 2007, related link here: http://tir.astro.utoledo.edu/jdsmith/code/cubism.php); spectra were extracted at the positions of these three knots from Spitzer-IRS Short-Low and Long-Low observations taken as part of Spitzer program 3310. The CUBISM spectrum of FMK 1 was input into the Exposure Time Calculator (ETC) to estimate integration times for MIRI MRS observations. As for the NIRSpec IFU, none of the 2MASS J, H, or K band images of the knots showed much continuum emission, so no continuum emission was assumed for estimating integration times for the NIRSpec IFU in the ETC. The integrated flux and central wavelengths of the line emission from 0.6–1.1 μm for FMKs 1, 2, and 3 were obtained from Table 2 of Hurford & Fesen (1996) and for FMKs 1 and 2 over 0.9–2.0 μm from Tables 2 and 3 from Gerardy & Fesen (2001). For both mid-infrared and near infrared lines, a line width of 4000 km/s was assumed, as this corresponded to the largest line widths of the lines observed by Spitzer-IRS (Ennis et al., 2006; Rho et al., 2008), and it slightly exceeds the velocity widths reported in Table 2 of Kilpatrick, C. D., et al., (2014). Both MIRI-MRS and the NIRSpec IFU have higher spectral resolution than the Spitzer-IRS high resolution modules, so if they resolve emission to be narrower than observed by Spitzer, to preserve flux, the lines would have to be stronger than assumed here, in which case even higher peak signal-to-noise (S/N) would be achieved in the line. The integration time in the ETC was estimated so that the peak value of S/N per pixel in the slice corresponding to the peak of any emission line of interest was > 14. This way, for the wavelength range between the half-power points in an emission line, the S/N per pixel at the peak pixel at any wavelength would be > 10 (i.e., $14 \times 2^{-0.5}$). This, in turn, would ensure the S/N per pixel for any pixel within a Half Width at Half Maximum (HWHM) of the peak pixel in a knot, within the half-power wavelength range of the emission line, would be > 5. S/N per pixel > 5 is needed to give confidence that the signal for a given pixel at a given wavelength slice is astronomical and not stochastic in nature. Thus, for all emission lines of interest, we expect S/N per pixel to be > 5 within a HWHM (spatially) of the center of each of the 3 knots, over the FWHM range (spectrally) of the emission line.

In the ETC, the sources (see JWST ETC Scenes and Sources Page Overview) were treated as extended sources with a 2-D Gaussian shape. The background level (see JWST Background Model) assumed did not seem to affect the required integration time much. “IFU Nod Off Scene” was chosen (see JWST ETC IFU Nod in Scene and IFU Nod off Scene Strategy); otherwise, each source’s signal would subtract from itself since the sources are all extended, and the resultant S/N calculation in the ETC would, as a result, be incorrect. For the MRS pointings toward the 3 knots and the dedicated MRS background, a MIRI-MRS exposure time of ~1665 seconds was required. In the ETC, this was achieved with 150 groups, 1 integration, and 4 exposures, in FAST readout mode. The 4 exposures in ETC roughly simulate the 4 dithers. FMKs 2 and 3 required less exposure time than FMK 1, but the total time cost for observing the three knots in separate observations versus as a single target group was similar, so by observing them as a target group, the detections for FMKs 2 and 3 will achieve higher S/N. In addition, according to the ETC, these integration times should be sufficient to obtain S/N > 5 in the 21 μm solid-state emission feature seen in the Ennis et al., (2006) spectra.

For our observations, the optimal wavelength setting for the NIRSpec IFU at the highest spectral resolution to obtain as many strong spectral lines as possible is the shortest wavelength setting using grating G140H and filter F070LP, which covers 0.95–1.2 μm. The NRSIRS2 readout pattern is used (see NIRSpec Detector Readout Modes and Patterns) to reduce readout noise. IRS2 readout patterns are useful for reducing 1/f noise (Rauscher et al., 2012). For the NIRSpec IFU observations, the targets were not combined as a target group; instead, they were made separate observations, as combining as a target group in this case increased the overall program time. In order to obtain S/N > 5 within the HWHM (spatially) of the peak pixel at each wavelength within the FWHM (spectrally) of as many of these lines as possible for each source, exposure times of 7936s, 3560s, and 3268s were needed for FMKs 1, 2, and 3, respectively. In the ETC, this comes from assuming the following numbers of groups/integrations/exposures, respectively: 27/1/4, 12/1/4, and 11/1/4. For the NIRSpec IFU ETC simulations, the 4 exposures simulate a 4-point dither pattern, like for the MRS ETC simulations.

Astronomer's Proposal Tool

> *See also: MIRI MRS APT Template, NIRSpec IFU Spectroscopy APT Template , JWST APT Science Parallel Observations*
>
> *Associated APT File: ifuprop14feb2018.aptx*

APT version 25.4.2 was used, and the program was checked in APT version 25.4.3. To save time on overheads, the 3 knots are made into a target group for MIRI-MRS. For the NIRSpec IFU observations, a 2 × 2 mini-mosaic is assumed (see Figure 1 and NIRSpec FS and IFU Mosaic APT Guide), with 10% overlap for both mosaic rows and columns, as the NIRSpec IFU field of view is 3” × 3”. The MIRI-MRS fields of view are increasingly larger for longer-wavelength channels, going up to near 8” × 8” for Channel 4, so a mini-mosaic is less important for the MRS than NIRSpec IFU. For the MRS, we obtain only 1 pointing per FMK plus a dedicated sky pointing (Figure 1). For the NIRSpec IFU, the 4-point small cycling dither pattern (see NIRSpec IFU Dither and Nod Patterns) is used at each of the 2 × 2 mosaic positions, while for MIRI-MRS, a 4-point extended dither pattern (see MIRI MRS Dithering) is used in the “positive” direction. All 3 grating settings are included for MIRI-MRS, to observe the entire 5-28 micron spectrum of each knot.

For each NIRSpec IFU observation, a single leakcal exposure (see NIRSpec MSA Leakage Correction for IFU Observations) was requested because of extended emission from Cas A incident upon the MSA quadrants for nearly any orient. Using APT, it was found that no more than about 6-7 stars brighter than K=11.5 were located within the MSA quadrants, for any given Aperture PA value. Assuming a typical star was K5 V in ETC, it was found that a contaminant star would have to be brighter than K=11.5 to be detected at S/N > 5 at any wavelength being observed, for the NIRSpec IFU exposure parameters. This is such a small number of stars that it is anticipated any pixels contaminated by their signal can be flagged and ignored during cube-building, though this ability to flag and remove pixels is currently not supported by the data reduction pipeline.

Simultaneous imaging with MIRI will allow deep imaging of nearby fields, which comes for free with the MRS observations. For MIRI imaging, the FAST readout mode is recommended, so we chose 150 groups and 1 integration (the same as for the MRS observations), with the same 4-point dither pattern as with the MRS. The simultaneous imaging for the background position will image all 3 FMKs, and the simultaneous imaging for the 3 knots will image a considerable portion of the north of Cas A. The F1130W filter was chosen for simultaneous imaging. It was determined in ETC that none of the 2MASS catalog sources observed in MIRI simultaneous imaging would cause even partial saturation.

No target acquisition was selected for either the MRS or the NIRSpec IFU, as blind pointing was judged to be sufficient for both cases.

Altogether, this program totals 36.9 hours of charged time, of which 25.8 hours are science time.

Figure 1: Mosaic Patterns

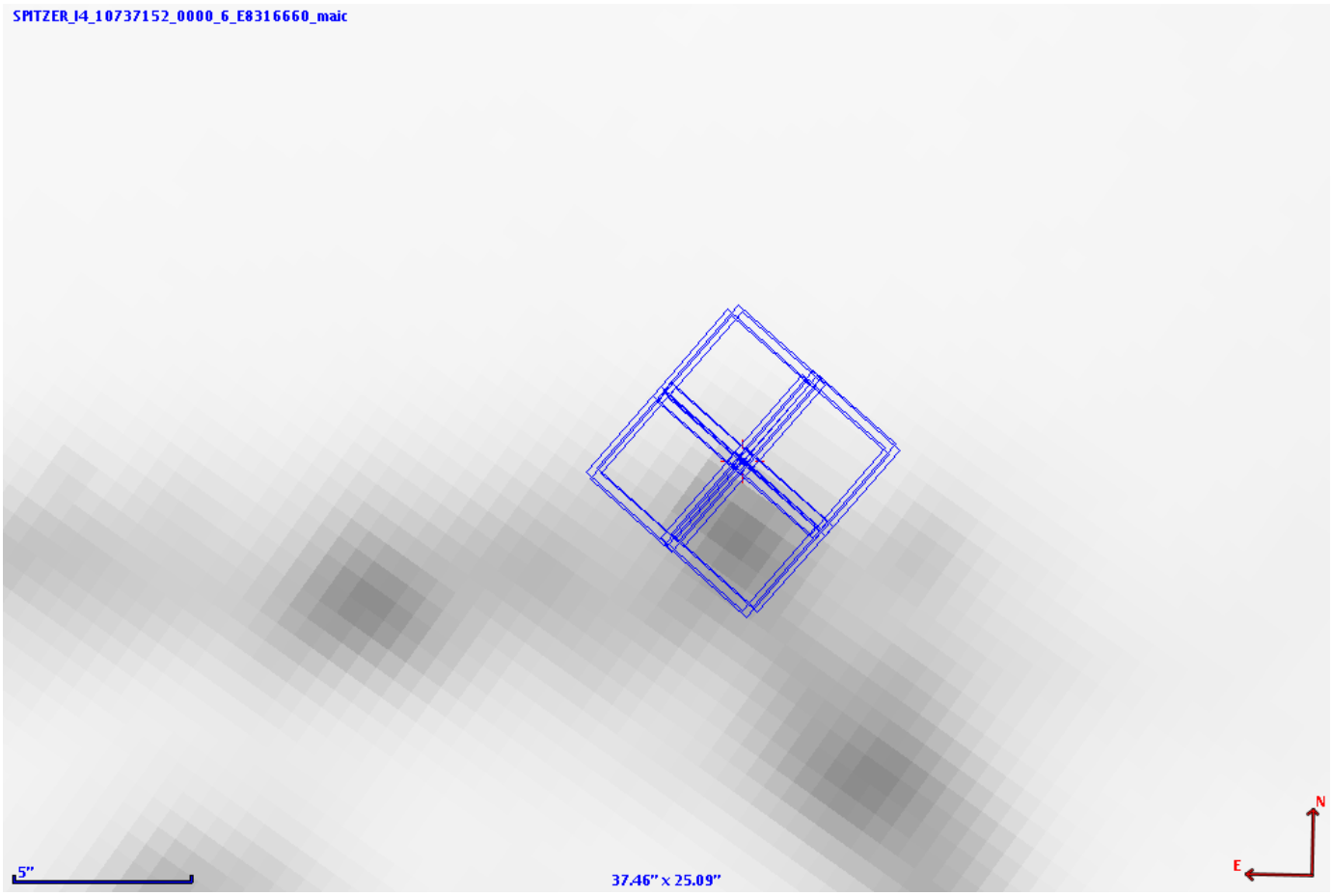

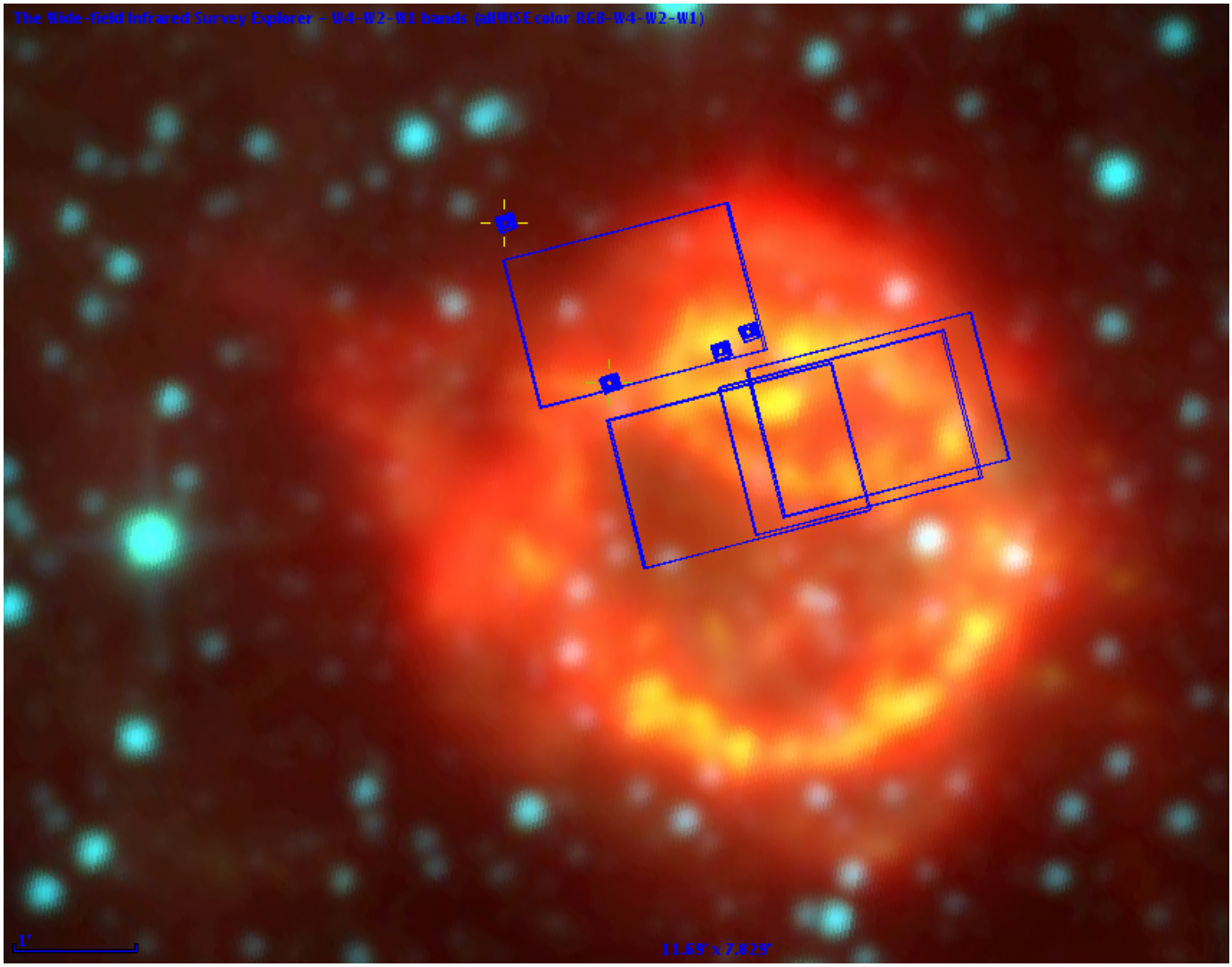

Top: 2 × 2 "mini-mosaic" pattern for NIRSpec IFU observations of FMK1, layered on top of an 8 m image from AOR 10737152 from Spitzer program id# 3310 (PI: L. Rudnick). Bottom: MIRI-MRS observations of FMK1, FMK2, FMK3, and the dedicated sky position, layered on top of a WISE three-color image. Also shown are the areas observed in simultaneous imaging with the MIRI imager. Screenshots from Aladin, generated from APT. The line segment in the lower-left corner of each image gives a length scale, which is 5 arcseconds for the Spitzer image and 1 arcminute for the WISE image. North is up, and East is to the left.

Associated files

APT File: ifuprop14feb2018.aptx

References

Boyer, M. L., et al., 2012, ApJ, 748, 40
The Dust Budget of the SMC: Are AGB Stars the Primary Dust Source at Low Metallicity?

Docenko, D., & Sunyaev, R. A., 2010, A&A, 509, A59
Fine-structure infrared lines from the Cassiopeia A knots

Douvion, T., et al., 2001, A&A, 369, 589
Dust in the Tycho, Kepler and Crab supernova remnants

Draine, B. T., 2009, ASP Conference Series, 414, 453
Interstellar Dust Models and Evolutionary Implications

Ennis, J. A., et al., 2006, ApJ, 652, 376
Spitzer IRAC Images and Sample Spectra of Cassiopeia A's Explosion

Fesen, R. A., et al., 1988, ApJ, 329, L89
Highest velocity ejecta of Cassiopeia A

Gerardy, C. L., & Fesen, R. A., 2001, AJ, 121, 2781

Spitzer IRAC Images and Sample Spectra of Cassiopeia A's Explosion

Houck, J., et al., 2004, ApJS, 154, 18
The Infrared Spectrograph (IRS) on the Spitzer Space Telescope

Hurford, A. P., & Fesen, R. A., 1996, ApJ, 469, 246
Reddening Measurements and Physical Conditions for Cassiopeia A from Optical and Near-Infrared Spectra

Kilpatrick, C. D., et al., 2014, ApJ, 796, 144
Interaction between Cassiopeia A and Nearby Molecular Clouds

Matsuura, M., et al., 2009, MNRAS, 396, 918
The global gas and dust budget of the Large Magellanic Cloud: AGB stars and supernovae, and the impact on the ISM evolution

Rauscher, B. J., et al., 2012, Proceedings of the SPIE, article 84531F
Reducing the read noise of HAWAII-2RG detector systems with improved reference sampling and subtraction (IRS 2)

Rho, J., et al., 2008, ApJ, 673, 271
Freshly Formed Dust in the Cassiopeia A Supernova Remnant as Revealed by the Spitzer Space Telescope

Smith, J. D. T., et al., 2007, PASP, 119, 1133
Spectral Mapping Reconstruction of Extended Sources

Werner, M. W., et al., 2004, ApJS, 154, 1
The Spitzer Space Telescope Mission

JWST technical documents